Citation for published version:
Al-Battal, NH, Cleaver, DJ & Gursul, I 2019, 'Unsteady actuation of counter-flowing wall jets for gust load attenuation', *Aerospace Science and Technology*, vol. 89, pp. 175-191. https://doi.org/10.1016/j.ast.2019.03.053

DOI:
10.1016/j.ast.2019.03.053

Publication date:
2019

Document Version
Peer reviewed version

Link to publication

Publisher Rights
CC BY-NC-ND

University of Bath

General rights
Copyright and moral rights for the publications made accessible in the public portal are retained by the authors and/or other copyright owners and it is a condition of accessing publications that users recognise and abide by the legal requirements associated with these rights.

Take down policy
If you believe that this document breaches copyright please contact us providing details, and we will remove access to the work immediately and investigate your claim.

Download date: 05. Jun. 2020

Unsteady Actuation of Counter-Flowing Wall Jets for Gust Load Attenuation

Nader H. Al-Battal, David J. Cleaver and Ismet Gursul

Department of Mechanical Engineering, University of Bath, Bath, BA2 7AY, UK

Counter-flowing wall jets actuated on the upper surface of an airfoil are investigated for the purpose of controlling gust encounters. For periodic and transient actuations, phase-averaged lift force and particle image velocimetry measurements are presented for a NACA 0012 airfoil, at a Reynolds number of 660,000, for a range of reduced frequencies and three jet locations, x_J/c = 0.08, 0.60 and 0.95. For periodic actuation, amplitude of lift oscillations decrease and phase delay increase with increasing reduced frequency. The effect of reduced frequency on the amplitude and phase is more significant for blowing locations near the leading-edge and with increasing angle of attack. Transient actuation reveals the slow response of the separated flow, and therefore lift, with the delay becoming more pronounced for blowing near the leading-edge. Estimated time constants are similar to previous observations for forced separation and reattachment.

Nomenclature

α		angle of attack
C_μ		momentum coefficient
$C_{\mu max}$		maximum momentum coefficient
C_L		lift coefficient
C_{Lmax}		maximum lift coefficient
C_{Lmin}		minimum lift coefficient
C_{Loff}		lift coefficient for no blowing
C_{Lon}		lift coefficient for continuous blowing
C_{Lmean}		mean lift coefficient
c	=	chord length
f	=	frequency
h_J	=	slot width
k	=	reduced frequency
κ	=	time constant
φ	=	phase angle
ρ	=	density
b	=	span
τ	=	normalized time, $U_\infty t/c$
x_J	=	location of jet
U_J	=	time-dependent jet velocity
U_∞	=	freestream velocity
Re	=	Reynolds number

I. Introduction

The structural weight of civil transport aircraft is often determined by critical load cases caused by positive gust loads. Furthermore, gusts are responsible for over a third of wind related accidents [1], and are detrimental to passenger comfort. The efficiency and performance of aircraft is therefore largely dependent on the ability to counter gust loads. Current gust load alleviation techniques consist of ailerons and spoilers. However, these devices are sized for maneuvers. Their large inertia means their effectiveness reduces with gust frequency. Highly responsive high-frequency actuation is fundamental to effective gust load alleviation [2, 3]. One possibility is a high-frequency mechanical device such as the mini-tab, a small mechanical surface deflected upwards near the trailing-edge [2, 3]. Mini-tabs located further upstream have been found to provide significant lift reduction [4].

A second possibility for high-frequency gust load alleviation is fluidic actuators developed for active flow control [5]. Blowing perpendicular to the airfoil surface near the trailing-edge [3, 6, 7] has been proposed. This concept is similar to conventional jet-flaps [8], however it is applied on the upper surface of the airfoil in order to decrease the lift. Even though the effectiveness of the blowing (with low momentum coefficients) perpendicular to the airfoil lower surface was demonstrated for lift increase [9], this method is not necessarily effective when applied on the airfoil upper surface, in particular at further upstream locations. Counter-flowing wall jets [10, 11] are more effective than blowing normal to the surface, in particular when the location of the jet is immersed in the separated flow over the airfoil. Existence of partially separated flows is a possibility in take-off and landing as well as during an unsteady maneuver. Again, upstream jet locations have been found more advantageous with increasing angle of attack. Counter-flowing

wall jets, generated by plasma actuators placed on the lower surface of an airfoil, have been previously used to produce a virtual flap effect at a low Reynolds number [12].

It is clear that static (continuous) actuation of counter-flowing wall jets causes various degrees of separated flows over the upper surface of the airfoil, depending on their location. Unsteady actuation and frequency response of these actuators will be affected by the separated flows over the airfoil. In the case of fully separated flow over an airfoil, it is known that there are large time delays in the response of the flow to unsteady excitation [13]. This seems to be a limiting factor in the closed-loop control of lift on a low aspect ratio wing with fully separated flow [14]. As the response of the separated flow to actuation is a limitation, one may expect some improvement as the actuator location is moved downstream as the size of the separated region becomes smaller. However, even for fully attached flow on the airfoil surface, we expect a time delay of the lift response to actuation. This is due to the change of circulation and associated vorticity shedding from the trailing-edge. For example, when there is a sudden change in angle of attack (hence, circulation), the lift achieves its steady-state value slowly, similar to the response of a first-order dynamic system. This is known as the Wagner effect [15], which is related to the shedding of vorticity and can be considered as a "wake effect".

As the unsteady response of lift is crucial for high-frequency gust alleviation, in this paper, we experimentally investigate the response of the lift force to periodic and transient actuation of counter-flowing wall jets on the airfoil upper surface. In Reference [11], we investigated the static actuation (continuous blowing) of the counter-flowing wall jets and compared with surface-normal blowing. This paper focusses on the unsteady actuation of the counter-flowing jets with periodic and transient waveforms. In this paper, we experimentally investigate the response of the lift force to periodic and transient actuation of counter-flowing wall jets on the airfoil upper surface. We

consider three jet locations along the upper surface (x_J/c = 0.08, 0.60, 0.95), a momentum coefficient of C_μ = 1.6% and reduced frequencies $k < 0.5$, which are comparable to gust frequencies on civil aircraft. Phase-averaged lift force and velocity field have been measured and discussed in detail. Only the lift force was considered in these experiments. This is due to the concept of the fluidic actuator, which will only be deployed for short intervals, and therefore the associated drag increase is not considered to be an important issue compared to the potential load alleviation for the wing.

II. Experimental Techniques

Experiments were performed in a low-speed closed-circuit wind tunnel at the University of Bath. The working section has a length of 2.77 m, height of 1.51 m and width of 2.12 m. The freestream velocity for the experiments performed was U_∞ = 20 ms^{-1}. Turbulence intensity was measured to be less than 0.5%. Experiments were performed with the symmetrical NACA 0012 airfoil due to the availability of relevant aerodynamic data. The Reynolds number for the experiments is Re = 660,000. The boundary layer was tripped through trip wires of 0.3 mm diameter fixed at x/c = 0.1 on both the surfaces of the airfoil. This location corresponds to the maximum surface velocity [16] for NACA 0012 airfoil at α = 0°. Baseline lift force measurements for the airfoil, with no blowing, demonstrated close agreement with the lift data of Jacobs & Sherman [17] as discussed by Al-Battal et al. [11]. The chord length was c = 500 mm and span was b = 1500 mm. There was a 5 mm clearance between the walls of the wind tunnel and airfoil. The experiments were carried out for angles of attack α = 0°, 5°, 8°, 10°, 13° and 16°. This is to observe the behavior for angles of attack ranging beyond the stall angle, which was 13 degrees.

In this study three jet locations were studied: x_J/c = 0.08, 0.60, and 0.95. The wing was made with two parts. The leading 0.725c was manufactured with a carbon fiber composite exterior, reinforced internally with aluminum alloy structure and Rohacell ® XT foam, see Fig. 1. This added greater stiffness whilst maintaining low mass. Plenum chambers for the jet were installed at x/c = 0.08 and 0.60. These chambers were constructed from aluminum tubes with square cross-section and had a length of 1.50 m and width of 0.022 m. A narrow slot with a width of 1 mm angled perpendicular to the surface was cut across the entire span. Due to the intricate internal design required for the jet at x_J/c = 0.95, the aft 0.275c was rapid prototyped with DuraForm ® PA plastic. In order to prevent warping of the plastic, the trailing edge section was separated into five interlocking parts. The interior of the rapid prototyped section acts a plenum chamber for the x_J/c = 0.95 jet. For all three jet locations, x_J/c = 0.08, 0.60 and 0.95, the inlet was positioned at the wing root. Porous polyethylene sheets of a 2 mm thickness were fitted beneath the wing surface at each location, which helped to maintain a relatively uniform jet velocity in the spanwise direction (maximum deviation of the mean jet velocity was 5%). This was checked for the maximum jet speed for continuous blowing at several spanwise locations for all slots. The counter-flowing jet was produced by the addition of a carbon fiber piece attached to the slot on the wing, see Fig. 1a. This piece extends 5 mm (1%c) from the slot in the upstream direction and protrudes 0.5 mm (0.1%c), as sketched in the inset of Figure 1(a). Time-averaged force measurements were performed to confirm that the protrusion did not influence the lift curve when the jet was not active [10, 11]. Slots that are not used were covered with tape to produce a smooth surface. The tape had thickness of 0.13 mm and width of 19 mm. This thickness is smaller than the diameter of the trip wire.

A. Hot-Wire Measurements

Hot-wire measurements were performed to quantify the jet exit velocity. The measurements were taken using a TSI® 1210 – T1.5 hot-wire anemometer, connected to a TSI® 1750 Constant Temperature Anemometer bridge and control resistor tailored to the hot-wire probe. A National Instruments with 16-bit analogue to digital converter module, NI-9205, amplified the voltage signal. The hot-wire probe was calibrated in a calibration rig with a Pitot tube. The pressure was recorded using a Digitron 2020P digital manometer connected to the Pitot tube. Hot-wire measurements were taken for 42 velocities within a range of 0 – 50 ms^{-1}. Using King's Law equation, a non-linear equation is determined to correlate the measured voltage values to the corresponding velocity. The mean jet velocity at 2 mm away from the wall (in the potential core) was calculated from 20,000 samples at 2 kHz for 59 equally distributed spanwise locations, and revealed a maximum deviation of 5%. These measurements were taken for the normal jet for convenience, before the small thin plate was inserted to generate the upstream blowing wall jet.

A bespoke valve system was used to create the unsteady jet actuation. The system comprised of compressed air at 6.5 bar from the University compressors split to two Ingersoll Rand ARO filter /regulators to stabilize the pressure. The two streams are then separated into two pairs of Enfield LS-V25s Proportional Pneumatic Control Valves to create four streams that are recombined at the wing inlet. Hot-wire measurements at the exit of each of the four valves were taken to ensure there was no lag between them. For periodic blowing, measurements were taken at the mid-span location for a range of reduced frequencies, $0 \leq k \leq 0.47$. A total of 100 blowing cycles were recorded at 5 kHz and subsequently phase-averaged. For periodic actuation of the counter flowing wall jets, the actuators were excited with a sinusoidal waveform. An example of

the measured jet velocity corresponding to this type of excitation is shown in Figure 2(a). The momentum coefficient is defined as:

$$C_\mu = \frac{h_J U_J^2}{\frac{1}{2} U_\infty^2 c}$$

where U_J is the jet velocity and U_∞ is the freestream velocity, and h_J= 0.5 mm for all three jet locations. The uncertainty in the momentum coefficient is determined as 2.6%, taking into consideration the uncertainties associated with the jet area, jet velocity and dynamic pressure. The maximum momentum coefficient during the blowing cycle is fixed at $C_{\mu,max}$ = 0.016. As the frequency of the jet actuation is increased, the valves had to be adjusted and calibrated to maintain a peak momentum coefficient of $C_{\mu,max}$ = 0.016.

For transient measurements, the excitation waveform was selected as a step function. The measured (output) jet velocity resembles the response of a first-order system, with a time constant of the actuator. An example of the output (measured jet velocity) corresponding to this type of desired velocity is shown in Figure 2(b). For the jet in Figure 2(b), i.e. x/c = 0.60, the jet velocity reaches 90% of the maximum value in less than two convective time units. It takes slightly longer when jet is turned off. In both cases it is much smaller than the response time of the separated flows. For transient jet measurements, a total of 400 cycles were used to produce a phase-averaged velocity time history.

B. Force Measurements

For dynamic force measurements, a FUTEK S-type load cell was used to measure the unsteady lift force. A total of 350 cycles were taken at a sampling rate of 5 kHz. The airfoil was rotated

manually and the angle of attack measured using a rotary encoder with a precision of ± 0.02°. The lift force measurement system was dynamically calibrated through an electromechanical shaker positioned perpendicular to the airfoil to excite it sinusoidally through a carbon fiber shaft positioned at the center of mass for the entire system. The FUTEK S-type load cell was placed between the shaker and the airfoil to quantify the input force. The airfoil was forced at a range of frequencies between 1 Hz $\leq f \leq$ 20 Hz, with 0.5 Hz intervals, at force magnitudes of ± 10 N, 25 N and 50 N. The amplitude ratio and phase angles were determined through averaging 100 cycles. The resonant frequency of the system was approximately 7.25 Hz, or k = 0.57. To avoid the resonance effects, we only present data for $k \leq 0.47$. With increasing frequency, the amplitude ratio slightly increased and the phase angle increased for our experiments for $k \leq 0.47$. The dynamic calibration data (amplitude and phase) were used to correct the load-cell output using the following procedure: post-processing in MATLAB was performed to determine the amplitude and phase angles from the signal. This process required the output signal to be assessed in the frequency domain, through a Fast Fourier Transform, where the phase and amplitude information were extracted. This information is revised using the dynamic force balance calibration data and reverted to the time domain, where the lift coefficient values are obtained.

A jet reaction force occurs when the unsteady jet is activated. In order to account for this force, force measurements were also taken with the jet activated in zero freestream velocity. However, the reaction force was small, but was still deducted from force measurements taken inside the wind tunnel. The reason for this is that the maximum momentum coefficient was 0.016 and the direction of momentum flux (along the wall) is not in the lift force direction.

Transient measurements were carried out for α = 10° at x_J/c = 0.08, 0.60 and 0.95. In the transient experiments, the jet is turned on and the jet velocity remained constant for five seconds,

which is equivalent to 200 convective time units. We also performed experiments by turning the jet off and measuring the unsteady lift force. Transient measurements were repeated over 20 cycles.

C. Particle Image Velocimetry Measurements

The flow field was measured using a 2D-PIV system to further enhance the understanding of the flow physics associated with the unsteady jet. An EverGreen 200 mJ 15 Hz Nd:YAG double-pulse dual laser was used to cover the airfoil upper surface at z/b = 0.6, as shown in Fig. 1. Uncertainty of the laser alignment was approximately ±1 mm. The freestream air was seeded with olive oil droplets, atomized using a six-jet atomizer. The mean size of the droplets was 1 μm, which was deemed to be appropriate according to the Stokes drag equation [18]. The glass floor of the wind tunnel allowed two TSI® PowerView™ CCD 8 MP cameras (3,312 x 2488 pixels) to be placed in a tandem configuration, 1200 mm below the plane of interest. The dual camera configuration allows covering the entire airfoil surface while maintaining a high vector resolution. The cameras were fitted with two Nikon AF 50 mm NIKKOR f/1.8D lenses. A TSI® LaserPulse 610034 synchronizer was used to synchronize the camera and laser with an external trigger. This allowed the cameras to capture images at specific moments in the phase cycle, determined by the LabView software. Processing of the PIV images was performed in the TSI® Insight 4G software, which made use of a recursive Fast Fourier Transform cross correlator. The interrogation window size was kept at 32 x 32 pixels, to produce a spatial resolution of 4 mm (0.8%c). A total of 450 image pairs were captured to be phase-averaged. A MATLAB® code was created to merge the two phase-averaged velocity fields and utilized a weighted average in the overlap region between the two cameras. Velocity measurements have an uncertainty of 3% of the freestream velocity. The laser reflection is accentuated through the upstream blowing strip, therefore data were

collected from 5.6 mm away from the strip surface. Everywhere else it is approximately 2.3 mm from the wall.

III. Results and Discussion

A. Periodic Actuation

Figure 2(a) illustrates the definitions used throughout this discussion. Included in this figure is the normalized velocity magnitude of the jet, using the left-hand y-axis, with the peak velocity occurring near the phase φ = 180°. Total harmonic distortion for Figure 2a is 27%. This is determined by finding the fundamental and harmonic frequencies through Fourier analysis and then calculating the harmonic distortion in MATLAB®. The lift coefficient is also plotted, with dashed lines using the right-hand y-axis. The horizontal dashed red lines show the k = 0 steady-state limits; blowing off at the top C_{Loff}, and blowing on C_{Lon} at the bottom. The difference $(C_{\mathrm{Loff}} - C_{\mathrm{Lon}})$ is therefore the lift change achievable in steady-state conditions. For unsteady conditions, C_{Lmax} and C_{Lmin} represent the maximum and minimum lift coefficients, respectively, while the mean value of the coefficients are symbolized by C_{Lmean}.

The effect of reduced frequency on C_{Lmin} and C_{Lmax} relative to the no blowing case, i.e. $(C_{\mathrm{Lmin}} - C_{\mathrm{Loff}})$ shown with dashed line and $(C_{\mathrm{Lmax}} - C_{\mathrm{Loff}})$ shown with solid line, are demonstrated in Figures 3, 4, and 5, for jet locations x_J/c = 0.95, 0.60 and 0.08. The differences shown in these figures were calculated from the phase-averaged lift coefficient, hence include the contributions from the fundamental frequency as well as the higher harmonics. The difference between the lines is the amplitude of the lift fluctuations. The value at k = 0 is the change in the lift coefficient with continuous blowing for each angle of attack. Figure 3 shows that, for x_J/c =

0.95, the change in the lift coefficient for static actuation (k = 0) decreases with increasing angle of attack. The corresponding flow fields for k = 0 have been discussed in detail elsewhere [11]. Figure 3(a) for $\alpha = 0°$ shows little deviation from zero in the difference between maximum lift coefficient and no blowing ($C_{\mathrm{Lmax}} - C_{\mathrm{Loff}}$), until k = 0.31. Beyond this reduced frequency, the maximum lift coefficient begins to decrease slightly. This departure from the static value appears to increase with angle of attack, except for the post-stall angle of attack of $\alpha = 16°$. As reduced frequency increases for all angles of attack, the minimum lift coefficient increases slightly or remains roughly constant at high angles of attack. The maximum and minimum lift coefficients converge to one another, indicating a reduction in the amplitude of the lift fluctuations with reduced frequency. Across the reduced frequencies considered, the mean lift coefficient experiences minimal change for all angles of attack.

Figure 4 presents the data for the jet at x_J/c = 0.60. It is seen that, in this case, the change in the lift coefficient for static actuation (k = 0) increases with angle of attack until the stall angle, and then drops off at the post-stall angle of attack. The maximum change in the lift coefficient occurs for the stall angle and is larger than that observed for x_J/c = 0.95. These features are due to the variations in the natural flow separation for the baseline case as well as the forced separation due to blowing as the angle of attack is varied. For periodic actuation, the effect of the reduced frequency is similar to the previous case of x_J/c = 0.95. The lift amplitude decreases with increasing reduced frequency for all angles of attack. It appears that the rate of the decrease with reduced frequency increases with angle of attack until the stall angle of attack is reached. Hence, the effectiveness of blowing for lift reduction decreases substantially with increasing frequency near the stall angle. The decrease of the rate with frequency slows down at the post-stall angle of attack α = 16° in Fig. 4(f).

When the jet is located at x_J/c = 0.08, Figure 5 shows that the change in the lift coefficient for static actuation (k = 0) is qualitatively similar to that of the case of x_J/c = 0.60. However, the effect of the angle of attack is more significant. The change is very small for $\alpha = 0°$, but reaches nearly $C_{Lmin} - C_{Lmax} \approx -0.5$ at the stall angle of attack, dropping again at the post-stall angle of attack. Similar to previous cases, the difference between the maximum and minimum lift coefficients decreases with increasing reduced frequency. In particular, at the stall angle of attack ($\alpha = 13°$) in Figure 5(e), both the maximum and minimum lift coefficients reveal significant changes at higher reduced frequencies, resulting in a rapid drop of the lift amplitude. It is worth noting that lift reduction with unsteady actuation is still possible at the post-stall angle of attack ($\alpha = 16°$) for this location of blowing (x_J/c = 0.08). This is in contrast to the observations for blowing locations further downstream. Manipulation of the naturally separated flow near the leading-edge seems effective in both static [11] and the dynamic cases.

Figure 6 summarizes the variation of the difference ($C_{Lmin} - C_{Lmax}$), or amplitude, as a function of reduced frequency for the angles of attack tested and the three jet locations. In terms of load (lift) alleviation capability, the effectiveness increases as the blowing location is moved upstream. Also, the effectiveness may increase or decrease with angle of attack, depending on the location of blowing. Generally, there is a decrease in the lift reduction with increasing reduced frequency. For x_J/c = 0.08 and 0.60, the rate of decay in amplitude appears to increase with increasing angle of attack until the stall angle is reached.

Presented in Figure 7 is the phase angle between the lift response and the measured jet velocity for locations x_J/c = 0.95, 0.60 and 0.08. As the lift decreases with blowing (increase in the jet velocity) for the quasi-state case (continuous jet), the phase angle at k = 0 is φ = -180° as indicated with the dashed lines to the first data point. When comparing the phase angle of the lift with respect

to the quasi-state case, for all three jet locations, it is apparent that the relative phase difference increases with increasing frequency as the jet location is moved upstream. Both effects (increasing frequency and upstream jet location) can be considered to be associated with increasing extent of the separated flows. Also, it is apparent that the effect of angle of attack is the largest for the most upstream blowing location. Increasing angle of attack is also associated with increasing extent of the separated flows. Therefore, the phase angle of the lift seems to increase with any parameter that makes the flow more separated.

Varying effects of the jet location and reduced frequency on the amplitude and phase angle of the lift are reflected in the hysteresis loops of the lift as a function of the blowing phase. The representative data are shown for $\alpha = 5°$ (pre-stall) in the left column and for $\alpha = 13°$ (stall angle) in the right column of Figure 8. All loops are clockwise. As the jet location is moved upstream, decreasing amplitude for the pre-stall and increasing amplitude for the stall angle are evident. For the pre-stall angle of attack, the hysteresis loops start with negative slope at low reduced frequency and then the slope decreases with the increasing reduced frequency. However, for the stall angle of attack, the loops may even gain positive slope at high reduced frequencies. In particular, for x_J/c = 0.08, even at low reduced frequencies, lift response is characterized by very large phase lags. As can be seen with k = 0.08, the phase difference is $\varphi \approx$ -100°, subsequently causing the hysteresis loop to transform into a box-like form. This highlights that there is a large delay in response before the upstream blowing jet is able to incite a change in the flow. The loops gain a positive slope with increasing frequency, due to the increasing phase lag, resulting in the lift decreasing with blowing intensity. Existence of these hysteresis loops and large phase delays are inherent in the massively separated flows near stall angle and at high reduced frequencies. Obviously, this is not desirable for control purposes but inevitable.

Differences in the phase-averaged velocity fields for $\alpha = 13°$ and k = 0.39 are presented in Figures 9, 10, and 11 for x_J/c = 0.95, 0.60 and 0.08 respectively, alongside the time-averaged velocity for no blowing and continuous blowing. Also shown are the associated lift and jet velocity. In Figure 9, for the no blowing case there is a small separated region starting at approximately x/c ≈ 0.70. Once the jet is activated in the continuous blowing case the separated region becomes larger, resulting in a change in the lift coefficient of ΔC_{L} ≈ -0.09. For periodic blowing, the maximum and minimum lift coefficients do not reach the corresponding values of the baseline case and continuous blowing. The smallest separated region and the maximum lift coefficient are observed at around φ = 90°. When the jet velocity is maximum (at φ = 180°), the separated region is not the largest, but earlier separation occurs at φ = 270° when the lift is near minimum. Generally, the amplitude of lift variation is small, which is in broad agreement with the flow field measurements.

For x_J/c = 0.60 in Figure 10, continuous blowing produces a large recirculation region, with flow appearing to separate upstream of the jet at x/c ≈ 0.25. This is caused by the jet flow impinging with oncoming flow to deflect it away from the airfoil surface. The high velocity region near the leading edge is reduced in size, therefore contributing to the lift reduction, with ΔC_{L} ≈ -0.23 for the continuous blowing. Again, phase-averaged flow fields for the periodic blowing exhibit separated regions with sizes in between those of the baseline case and the continuous blowing. At the beginning of the cycle, φ = 0°, lift coefficient is near its minimum value. The recirculation region is reduced relative to continuous blowing. Subsequently, as lift returns to the maximum lift coefficient, wake size begins to reduce at φ = 180°, when the jet velocity is maximum. Hence, there is a very large phase lag, almost 180° (see also Figure 7).

For x_J/c = 0.08 in Figure 11, continuous blowing forces separation to occur immediately at this location, deflecting the shear layer away from the surface at a larger angle to that seen with x_J/c = 0.60. The combination of the larger recirculation region and deflection of the shear layer causes the largest change in lift coefficient observed throughout the cases considered, $\Delta C_L \approx$ -0.48. Minimum lift coefficient for periodic blowing occurs near φ = 60°, despite the jet velocity not being maximum at this phase. In fact, Figure 7 shows that there is a very large phase lag in this case. The flow fields show the separated region grows between φ = 0° and 90° in agreement with the lift measurements. Flow near the leading-edge accelerates at φ = 180°, with the separated region becoming even smaller at φ = 270° and the lift becoming maximum in between the two phases (at around φ = 230°).

B. Transient Actuation

To further understand the development of the phase-averaged lift and flow during a step-like actuation, Figures 12, 13 and 14 present the data for $\alpha = 10°$ and $C_{\mu,max}$ = 1.6% for x_J/c = 0.95, 0.60 and 0.08, respectively. The jet velocity measured by the hot-wire probe shows that it reaches the maximum velocity very quickly (within one convective time unit) in terms of the convective time scale, $\tau = U_\infty t/c$, once the jet is activated at $\tau = 0$. The flow fields are shown at various instants. In Figure 12 for x_J/c = 0.95, the flow field at a convective time of τ = -10 is representative of the baseline case. There is a small separated region near the trailing-edge in this case. After the activation of the jet, the separated region grows and reaches a steady-state between $\tau = 6$ and 9, which is in broad agreement with the lift time history.

For x_J/c = 0.60 in Figure 13, the final separated region is larger and the response of the flow is slower. The time taken to reach the steady-state lift is roughly $\tau = 20$. After $\tau = 10$, the changes in the flow fields are smaller. Again, the lift and flow measurements are consistent. For x_J/c = 0.08 in Figure 14, the final separated region covers roughly the whole airfoil surface. The lift time history suggests that it takes approximately 20 convective time units to reach the steady-state value. An interesting feature of the lift in this case is the initial increase and the peak around $\tau \approx 5$ following the activation of the jet at $\tau = 0$. Similar observations were made for a separated flow over a flat-plate flap, following the termination of the excitation Darabi & Wygnanski [13]. The initial overshoot, which also occurred around $\tau \approx 5$ in their case, was attributed to the formation of a large vortex over the flap. The time to reach the steady-state force was around τ = 20 to 30, depending on the angle of attack of the flap. Qualitatively similar observations were made in the reattachment process after the excitation is started [19], with the initial overshoot occurring around $\tau \approx 3$ and the reattachment time around τ = 20. The development of the flow field in Figure 14 is in agreement with the lift data. Surprisingly the separation point is still downstream of the jet slot at τ = 5 and is seen to reach the jet slot location after τ = 10. The fully developed flow is only attained around τ = 15.

In order to understand why the flow separation is so slow to respond, close-up images of local flow near the leading edge are presented in Figure 15 for τ = -10, 5, 10, 15 and 60. Figure 16 shows the corresponding vorticity plots for the same instants. Given that the slot exit is 0.5 mm (0.1%c), the boundary layer upstream of flow separation is thin, and the reflections near the wall exist, the details of the interaction of the wall-jet with the approaching boundary layer and the initial separation on the wall cannot be resolved. However, the development and growth of the flow separation as well as the lift-off of the shear layer from the surface are captured in Figures 15

and 16. Figures 15(a) and 16(a) show the initial state of the flow prior to the activation of the jet, with no sign of vorticity. For $\tau = 5$, slight changes in the velocity field are observed for $x/c \geq 0.15$ where a velocity reduction occurs. The vorticity plot for the same instant captures weak vorticity off the surface. As time increases to $\tau = 10$, the flow separation starting upstream of the counter-flowing jet becomes apparent, in particular in the vorticity plot (Figure 16(c)). For $\tau \geq 15$, the separated flow is fully developed. In summary, the forced separation process has inherently large relaxation time and there is a trend of slight increase of the separation time with the size of the final separated region.

We also carried out experiments for the reattachment process. The counter-flowing jet was turned off at $\tau = 0$ as shown in the example in Figure 17 for $x_J/c = 0.08$ and $\alpha = 10°$. As the jet velocity diminishes, there is an oscillation of the jet velocity. However, the effect of this oscillation is not observable in the lift response or flow fields. There is an overshoot of the lift in the opposite direction before it starts to increase. This is similar to the observations for the forced separation case shown in Figure 14. The time that takes to reach the steady-state case is still around 20 convective time units, which is also similar to the forced separation case. The similarities between our results and those of Darabi and Wygnanski [13, 19] for a flat-plate flap are striking. The velocity fields in Figure 17 reveal the slow process of reattachment of the flow.

As discussed earlier, the lift requires a long time (of the order of 10-20 convective time units) to reach the steady-state value. A better, more quantitative and more useful measure is the time constant, where the lift is approximated as the response of a first-order system. With this idealization, the time constant κ can be estimated from the response of the lift to a step or ramp input. The details of the curve fitting procedure are the same as Heathcote [20] proposed. Normalized time constants of various transient cases tested at different angles of attack and for jet

locations x_J/c = 0.08, 0.60 and 0.95 are shown in Figure 18. There is a trend of increasing $\kappa U_\infty/c$ with increasing angle of attack, whereas the effect of blowing location is weaker. Also, the time constants for the forced separation (jet turned on) and reattachment (jet turned off) are similar. It is worth noting that a different method of altering the lift by dynamic deployment of a mini-tab located at x/c = 0.85 for forced separation and reattachment also provided similar estimates of the time constant [21]. These observations are in broad agreement with the data for a flat-plate flap of Darabi and Wygnanski [13,19], who observed similar force responses for forced separation and reattachment.

IV. Conclusions

Phase-averaged lift force and two-dimensional PIV measurements were performed for unsteady actuation of counter-flowing wall jets employed on the upper surface of a NACA 0012 airfoil in order to study their capability for gust load attenuation. Although the change in the lift coefficient for continuous blowing (k = 0) depends on the chordwise location of blowing and the angle of attack, the effect of reduced frequency is similar for all cases. A reduction in the amplitude of the lift oscillations with increasing reduced frequency is observed. The rate of decay in the lift amplitude depends on the angle of attack and the location of the jet slot. Also, increasing phase lag of the lift has been observed with more separated flows, i.e. with increasing angle of attack and for upstream locations of the jet. These unsteady effects may result in the lift decreasing with increasing blowing intensity in the cycle. The large phase delays in the lift are consistent with the delays observed in the phase-averaged flowfields.

When a step-like variation of the jet velocity is employed, transient PIV measurements demonstrate that the separated region grows slowly, in agreement with the force data. With

increasing size of the separated region in the final state (for upstream locations of blowing), the response of the flow and lift force becomes slower. PIV measurements reveal the slow lift-up of the boundary layer vorticity as the wall jet interacts with the oncoming flow and separated wake. Estimated time constants for turning the jet on or off are similar, and increase with increasing angle of attack. Magnitude of the time constants as well as the general response of the flows are similar to those of other experiments on the forced separation and reattachment.

High-frequency actuation is necessary for effective gust load alleviation. However, using unsteady actuation has inherent limitations. Generality of these observations imply that the limitation is due to the response of the separated flows to any unsteady actuation. The gust load alleviation becomes more limited if the flow is more separated, i.e. with increasing angle of attack and for upstream locations of the jet.

Acknowledgments

The authors would like to acknowledge the support from an EPSRC studentship, Airbus UK, an EPSRC strategic equipment grant (EP/K040391/1 & EP/M000559/1) and EPSRC project (EP/M022307/1).

References

[1] Federal Aviation Administration, "Weather-Related Aviation Accident Study 2003-2007," 2010

[2] Heinz, J., Sørenson, N. N., Zahle, F., "Investigation of the Load Reduction Potential of Two Trailing Edge Flap Controls Using CFD," *Wind Energy*, Vol. 14, No, 3, 2011, pp. 449-462.

[3] Blaylock, M., Chow, R., Cooperman, A., and van Dam, C. P., "Comparison of Pneumatic Jets and Tabs for Active Aerodynamic Load Control," *Wind Energy Journal*, Vol. 17, No. 9, 2014, pp. 1365-1384.

[4] Heathcote, D., Gursul, I., and Cleaver, D., "Aerodynamic Load Alleviation Using Mini-tabs", *Journal of Aircraft*, DOI: 10.2514/1.C034574

[5] Cattafesta, L.N. and Sheplak, M., "Actuators for Active Flow Control", *Annual Review of Fluid Mechanics*, vol. 43, 2011, pp. 247-272.

[6] Boeije, C. S., de Vries, H., Cleine, I., van Emden, E., Zwart, G. G. M., Stobbe, H., Hirschberg, A., and Hoeijmakers, H. W. M., "Fluidic Load Control for Wind Turbine Blades," 47th *AIAA Aerospace Sciences Meeting Including The New Horizons Forum and Aerospace Exposition*, AIAA Paper 2009-684, 2009, pp. 1-8.

[7] Widjanarko, S. M. D., Geesing, I. J. A. K., de Vries, H. and Hoeijmakers, H.W.M., "Experimental/Numerical Investigation Airfoil with Flow Control by Synthetic Jets," *28th Congress of the International Council of the Aeronautical Sciences*, ICAS 2012-3.7.5, ICAS, Brisbane, 2012.

[8] Spence, D. A., "The Lift Coefficient of a Thin, Jet-Flapped Wing," *Proceedings of the Royal Society of London. Series A, Mathematical and Physical Sciences*, Vol. 238, No, 1212, Dec. 1956, pp. 46-68.

[9] Traub, L. W., Miller, A. C., and Rediniotis, O., "Comparisons of a Gurney and Jet Flap for Hingeless Control," *Journal of Aircraft*, Vol. 41, No. 2, 2004, pp. 420-423.

[10] Al-Battal, N., Cleaver, D., and Gursul, I., "Aerodynamic Load Control through Blowing," *54th AIAA Aerospace Sciences Meeting*, AIAA Paper 2016-1820, San Diego, 2016.

[11] Al-Battal, N., Cleaver, D., and Gursul, I., "Lift Reduction by Counter Flowing Wall Jets", *Aerospace Science and Technology*, vol. 78, 2018, pp. 682-695.

[12] Feng, L.H., K.S. Choi, and Wang, J.J., "Flow Control over an Airfoil Using Virtual Gurney Flaps", *Journal of Fluid Mechanics*, vol. 767, 2015, pp. 595-626.

[13] Darabi, A., and Wygnanski, I., "Active Management of Naturally Separated Flow over a Solid Surface. Part 2. The separation process", *Journal of Fluid Mechanics*, Vol. 510, 2004, pp.131-144.

[14] Kerstens, W., Pfeiffer, J., Williams, D., King, R., and Colonius, T., "Closed-Loop Control of Lift for Longitudinal Gust Suppression at Low Reynolds Numbers," *AIAA Journal*, Vol. 49, No. 8, 2011, pp. 1721-1728.

[15] Wagner, H. A., "Über die Entstehung des Dynamischen Auftriebes von Tragflügeln," *Journal for Applied Mathematics and Mechanics*, Vol. 5, Feb. 1925, pp. 17–35. doi:10.1002/zamm.19250050103

[16] Abbott, I. H., and von Doenhoff, A. E., *Theory of Wing Sections: Including a Summary of Airfoil Data*¸ Dover Publications, Inc., New York, 1959, pp. 321.

[17] Jacobs. E. N., and Sherman, A., "Airfoil Section Characteristics as Affected by Variations of the Reynolds Number," NACA Report 586, 1937, pp. 227-267.

[18] Prasad, A. K., "Particle Image Velocimetry," *Current Science*, Vol. 79, No. 1, 2000, pp. 51-60.

[19] Darabi, A., and Wygnanski, I., "Active Management of Naturally Separated Flow over a Solid Surface. Part 1. The forced reattachment process", *Journal of Fluid Mechanics*, Vol. 510, 2004, pp.105-129.

[20] Heathcote, D.J., “Mini-tabs for Aerodynamic Loads Alleviation”, PhD Thesis, University of Bath, 2017.

[21] Heathcote, D., Gursul, I., and Cleaver, D., “Dynamic Deployment of a Mini-tab for Aerodynamic Load Control”, in preparation for publication.

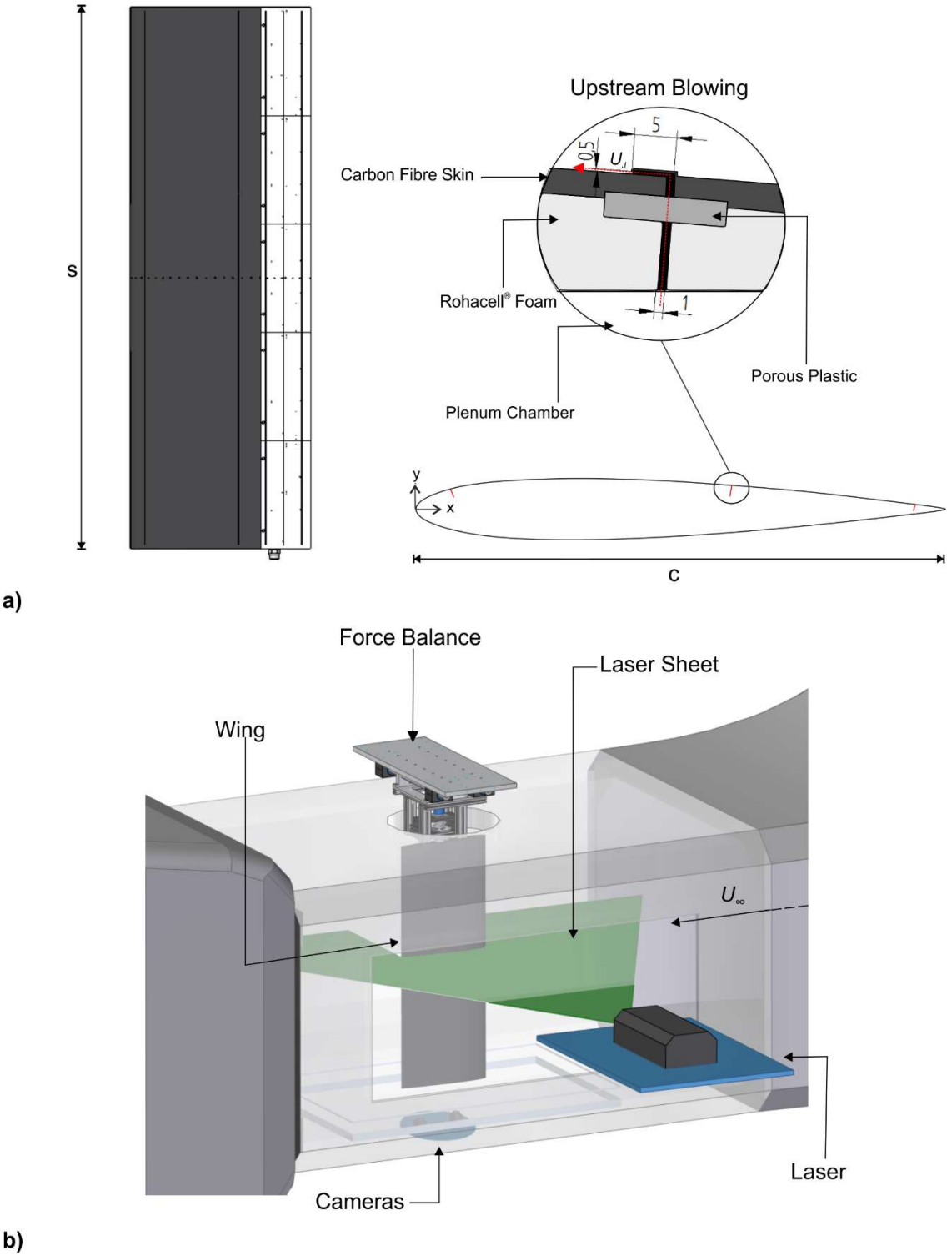

Figure 1. a) Schematic of the wing and jet slot; b) Experimental setup.

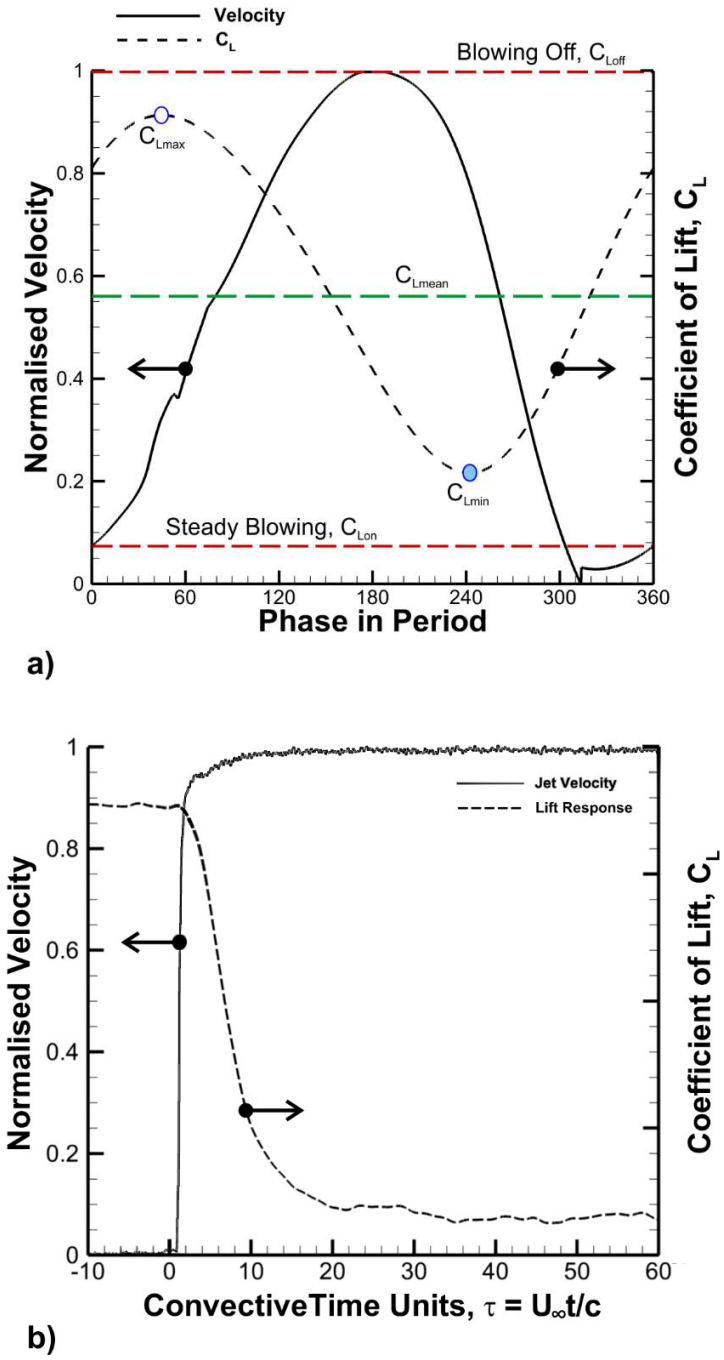

Figure 2. Examples of measured jet velocity and lift variation for a) periodic actuation, *x/c* = 0.95, *k* = 0.31, Cμ = 1.6%, α = 0 deg, b) transient actuation, *x/c* = 0.60, α = 10 deg.

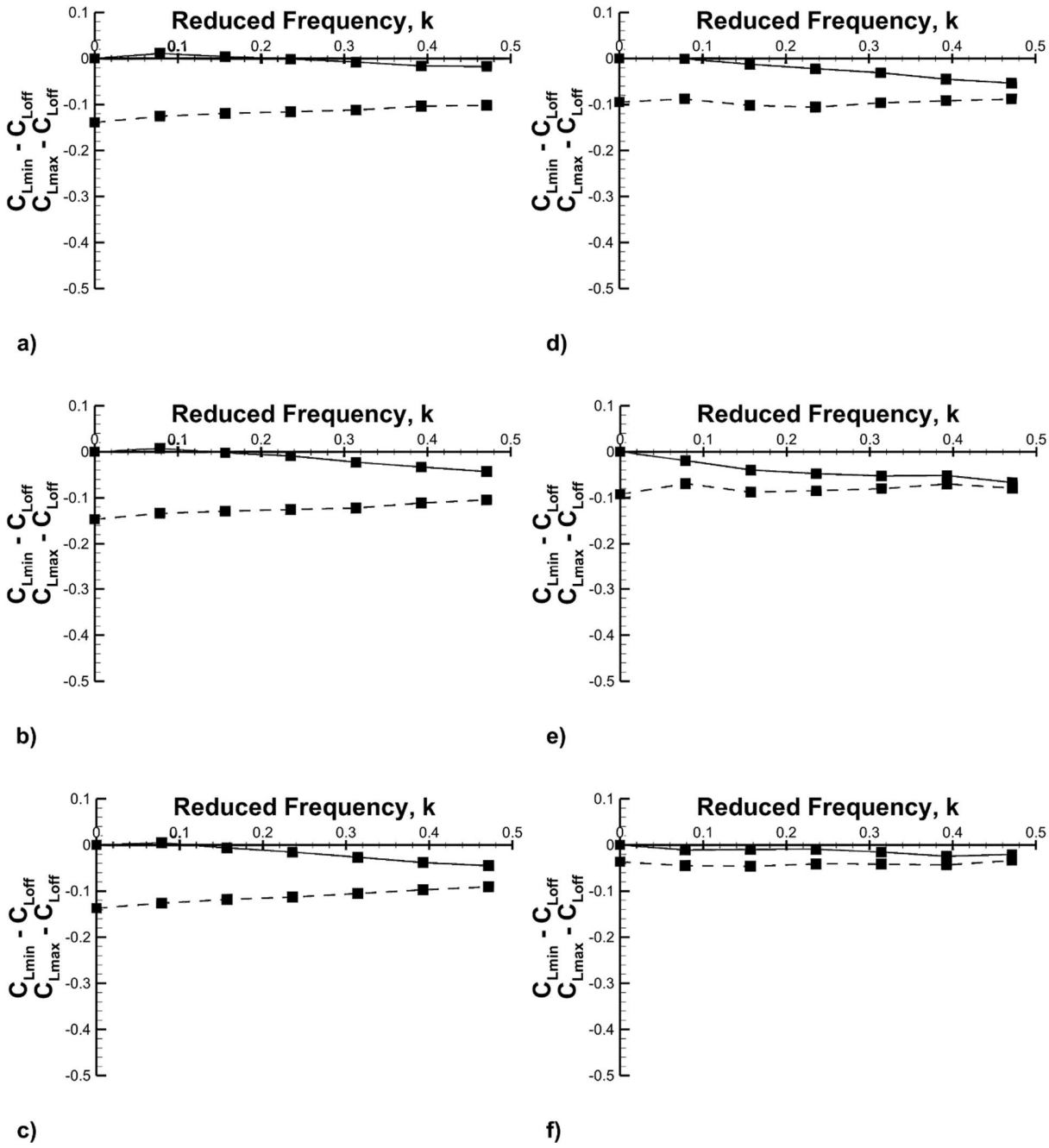

Figure 3. Variations of $(C_{\mathrm{Lmin}} - C_{\mathrm{Loff}})$ and $(C_{\mathrm{Lmax}} - C_{\mathrm{Loff}})$ with reduced frequency for x_j/c = 0.95 at a) α = 0°, b) α = 5°, c) α = 8°, d) α = 10°, e) α = 13° & f) α = 16°.

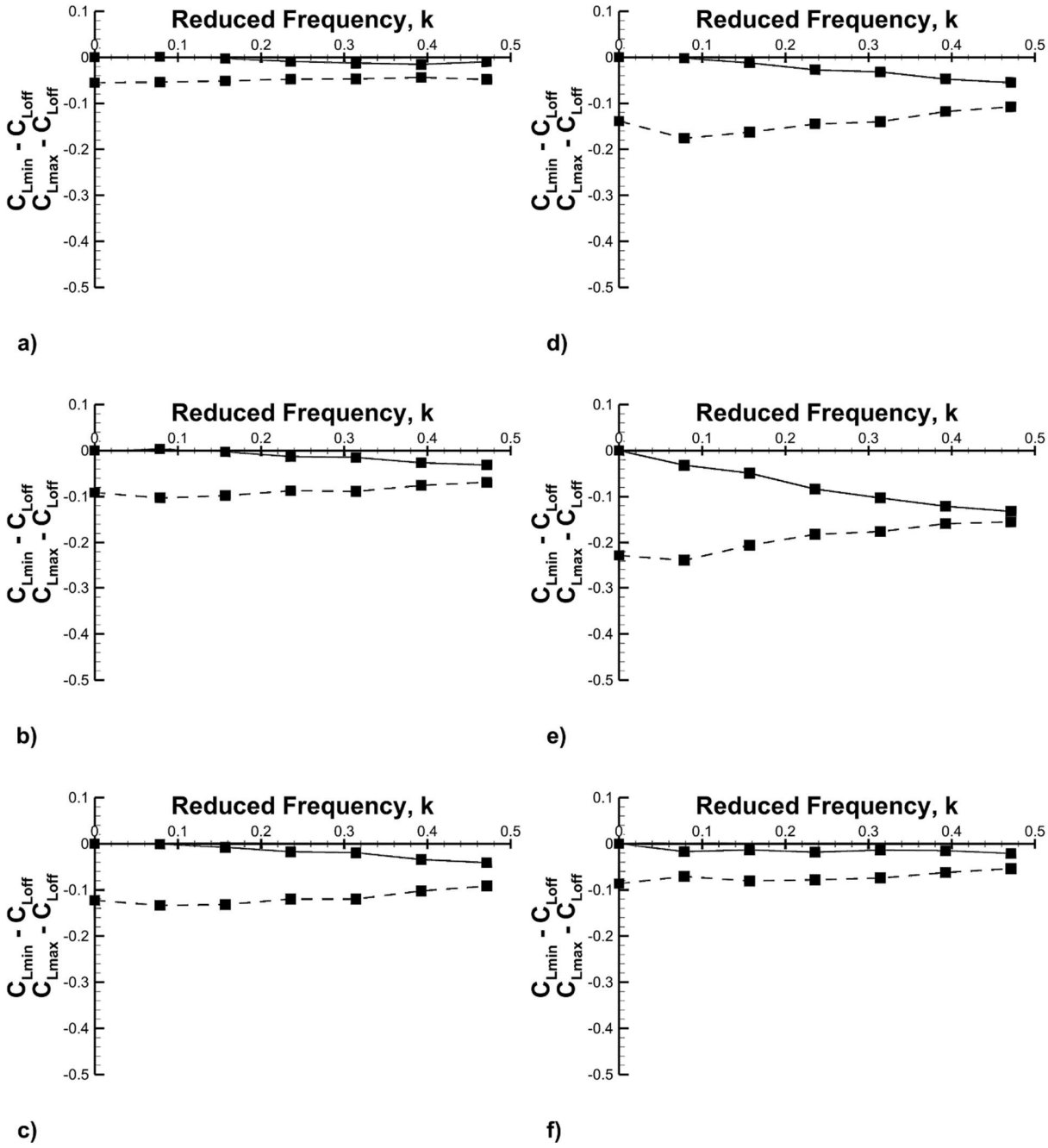

Figure 4. Variations of $(C_{\mathrm{Lmin}} - C_{\mathrm{Loff}})$ and $(C_{\mathrm{Lmax}} - C_{\mathrm{Loff}})$ with reduced frequency for x_j/c = 0.60 at a) α = 0°, b) α = 5°, c) α = 8°, d) α = 10°, e) α = 13° & f) α = 16°.

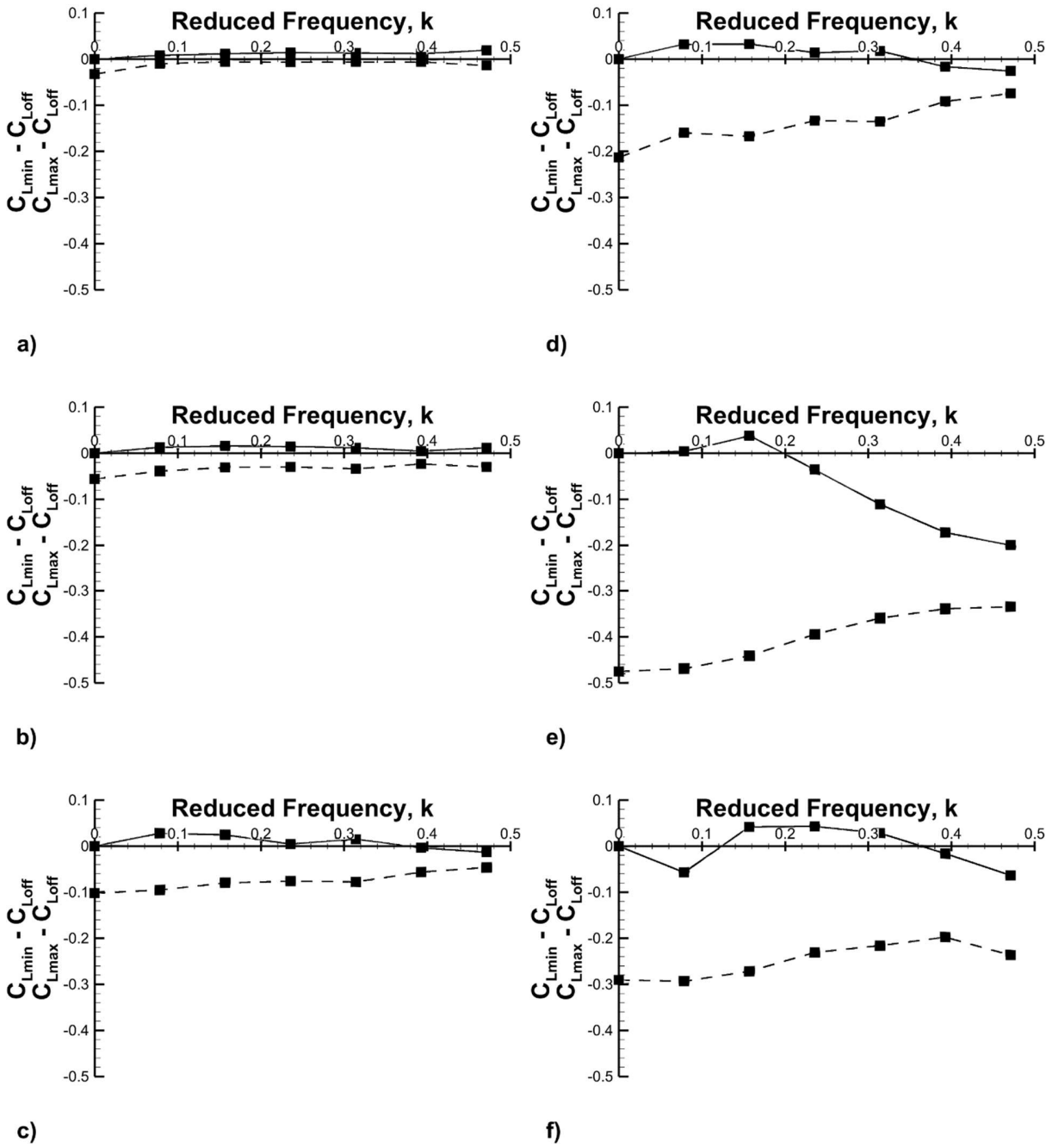

Figure 5. Variations of $(C_{\mathrm{Lmin}} - C_{\mathrm{Loff}})$ and $(C_{\mathrm{Lmax}} - C_{\mathrm{Loff}})$ with reduced frequency for x_j/c = 0.08 at a) α = 0°, b) α = 5°, c) α = 8°, d) α = 10°, e) α = 13° & f) α = 16°.

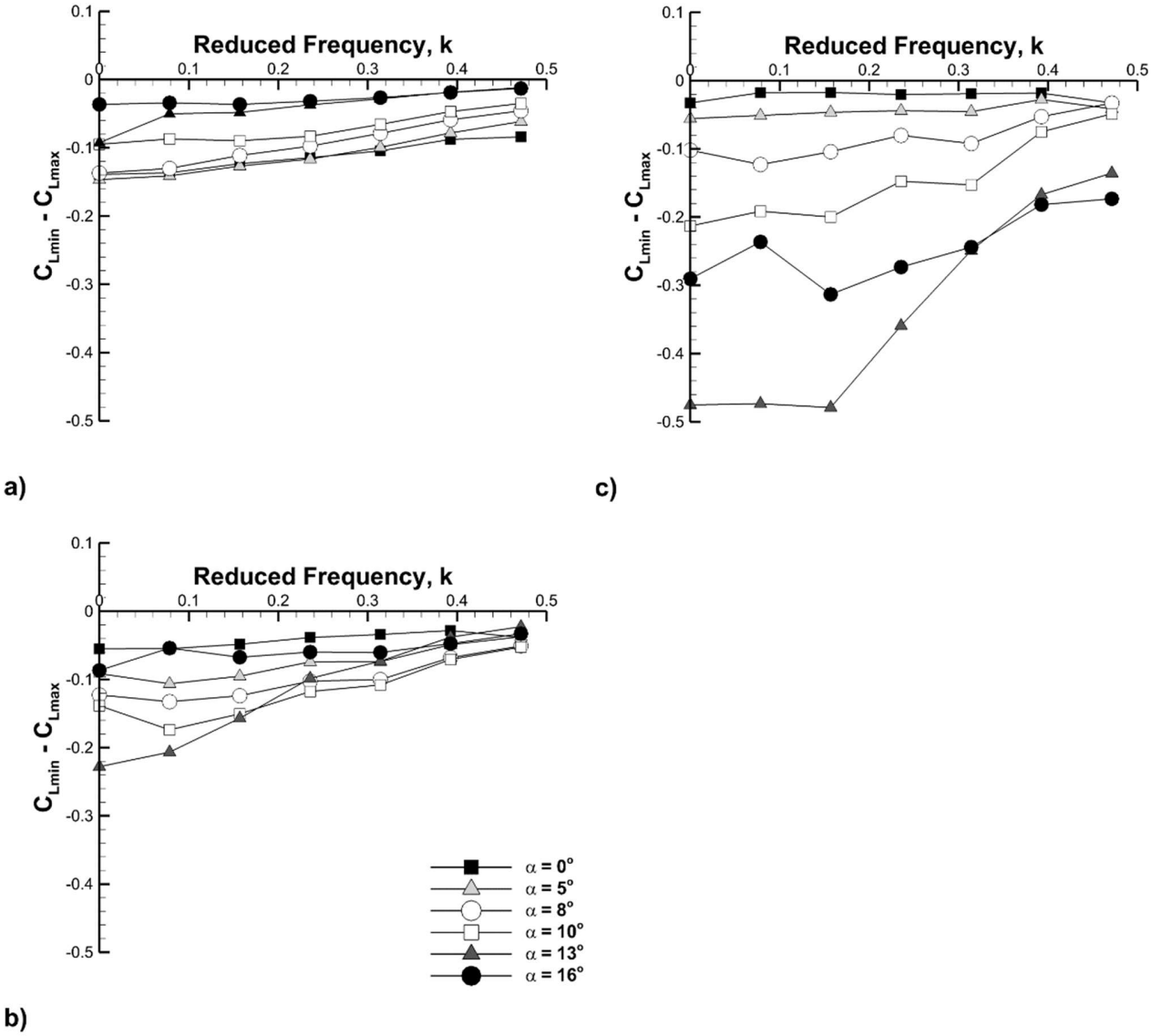

Figure 6. Variation of ($C_{Lmin} - C_{Lmax}$) with reduced frequency for a) x_j/c = 0.95, b) x_j/c = 0.60 & c) x_j/c = 0.08.

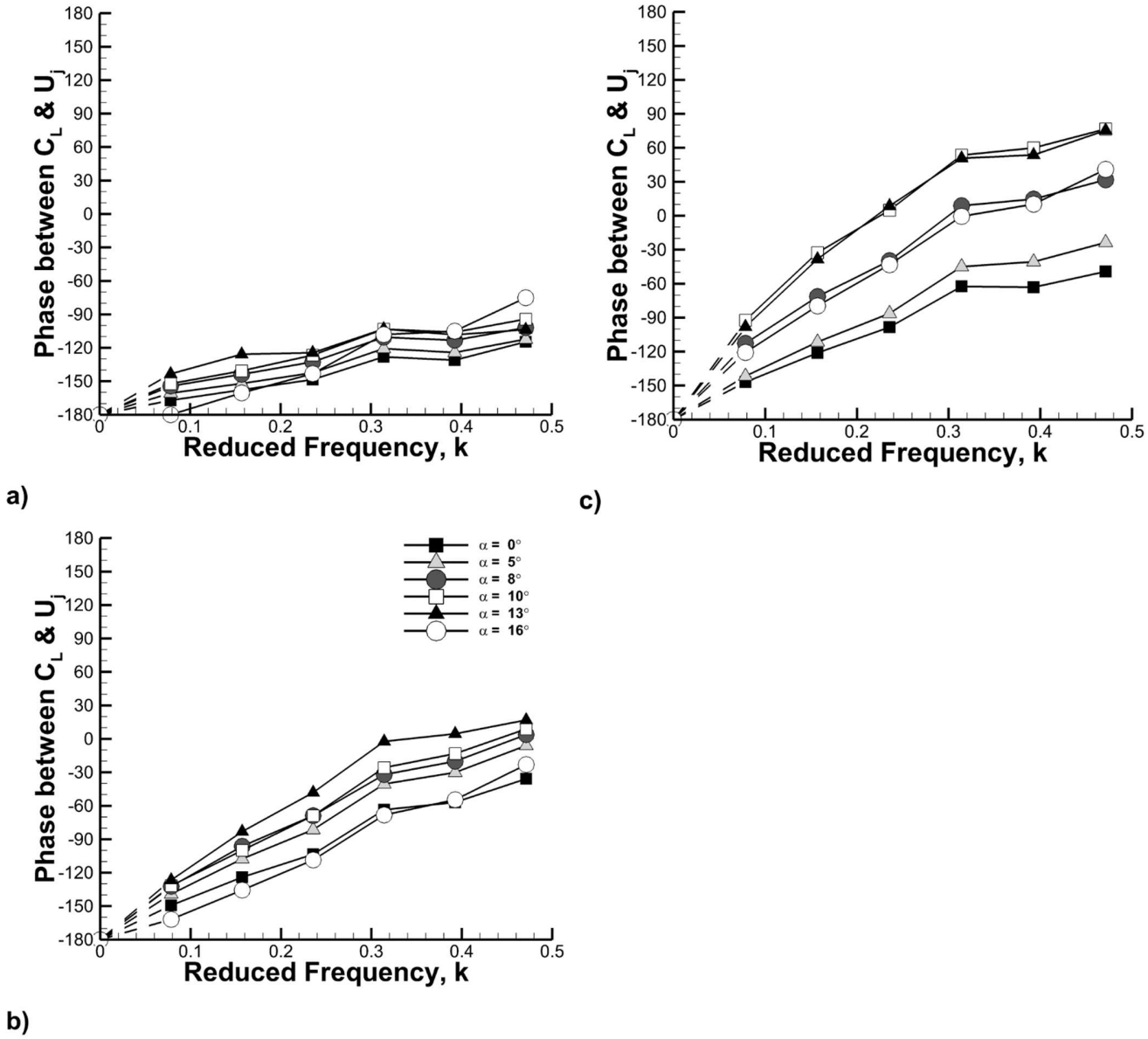

Figure 7. Variation of phase angle between lift coefficient and jet velocity at varying angles of attack for a) x_j/c = 0.95, b) x_j/c = 0.60 & c) x_j/c = 0.08.

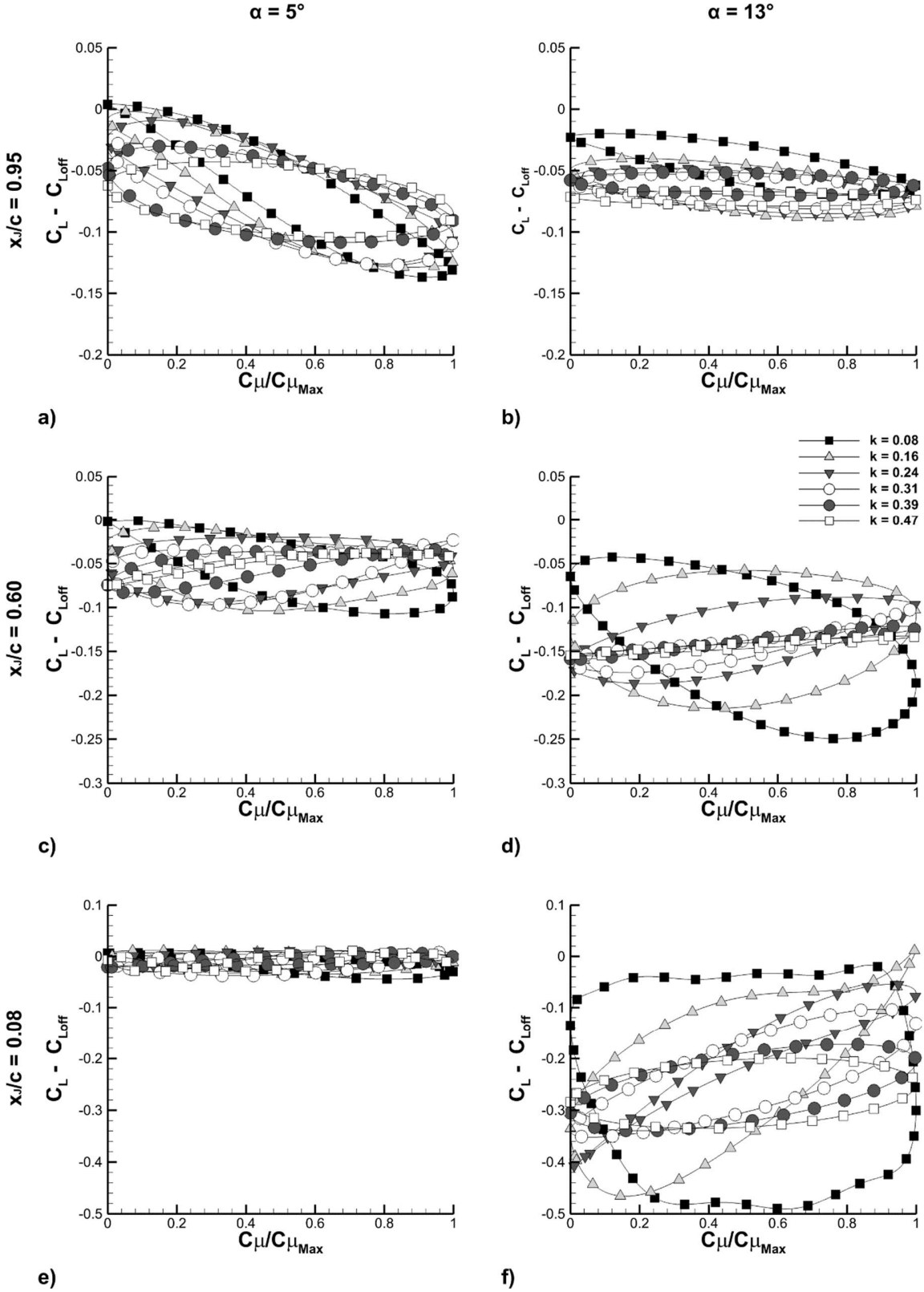

Figure 8. Phase-averaged loops of lift versus momentum coefficient for x_j/c = 0.95, a) α = 5° and b) α = 13°; x_j/c = 0.60, c) α = 5° and d) α = 13°; x_j/c = 0.08, e) α = 5° and f) α = 13°. All loops are clockwise.

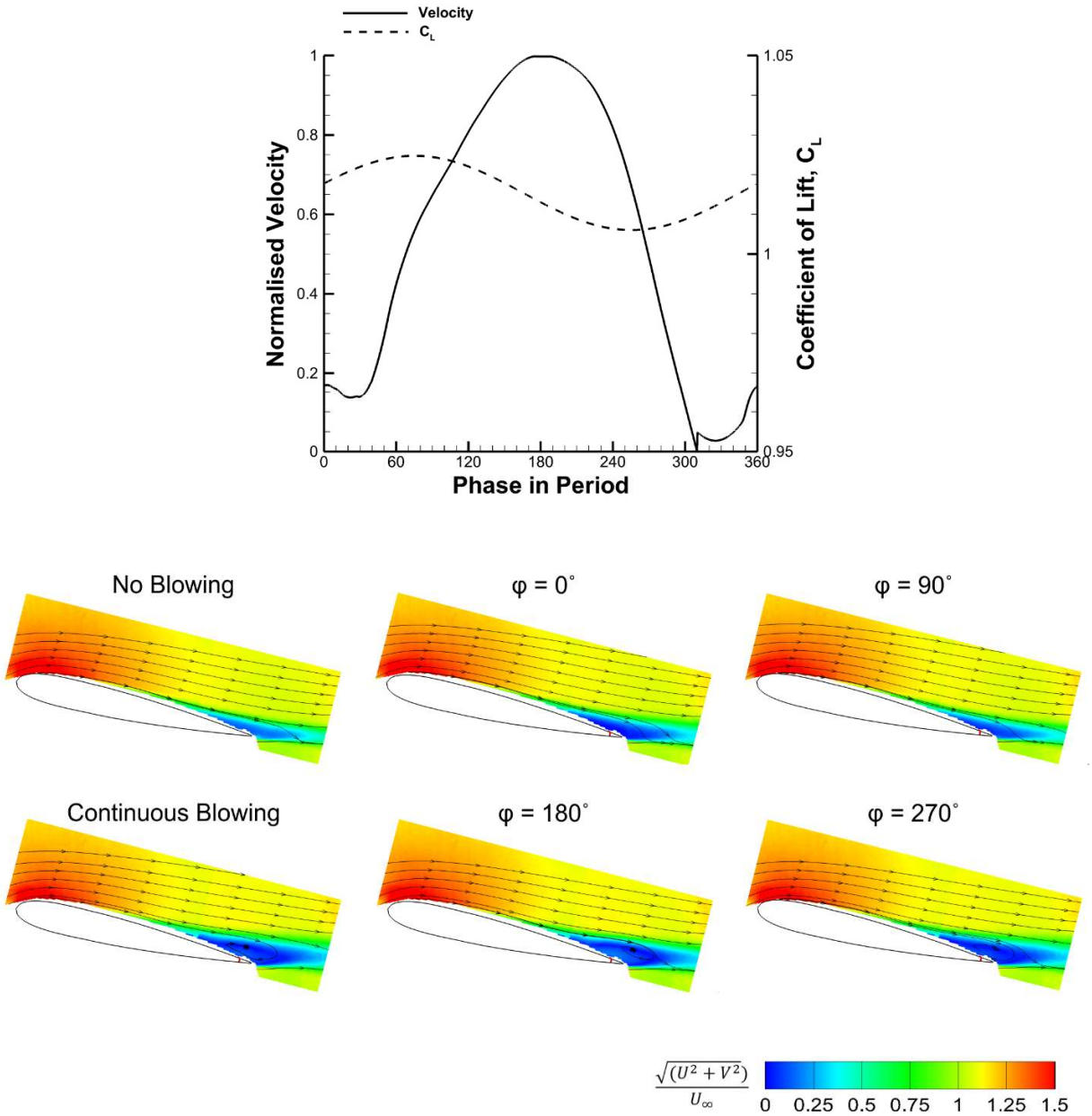

Figure 9. Phase-averaged velocity magnitude and streamlines at varying phases for k = 0.39, x_j/c = 0.95, and α = 13°.

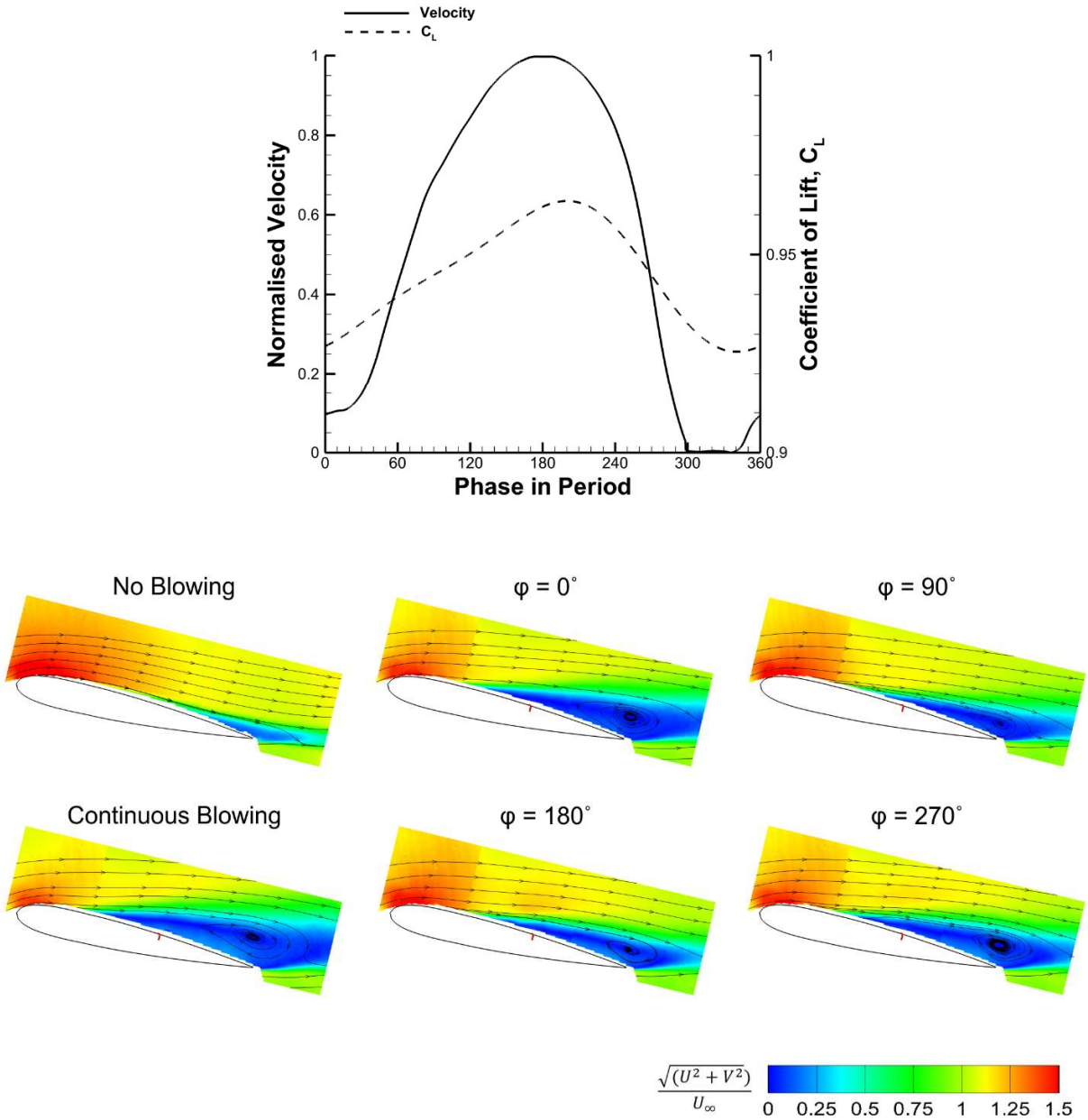

Figure 10. Phase-averaged velocity magnitude and streamlines at varying phases for k = 0.39, x_j/c = 0.60, and α = 13°.

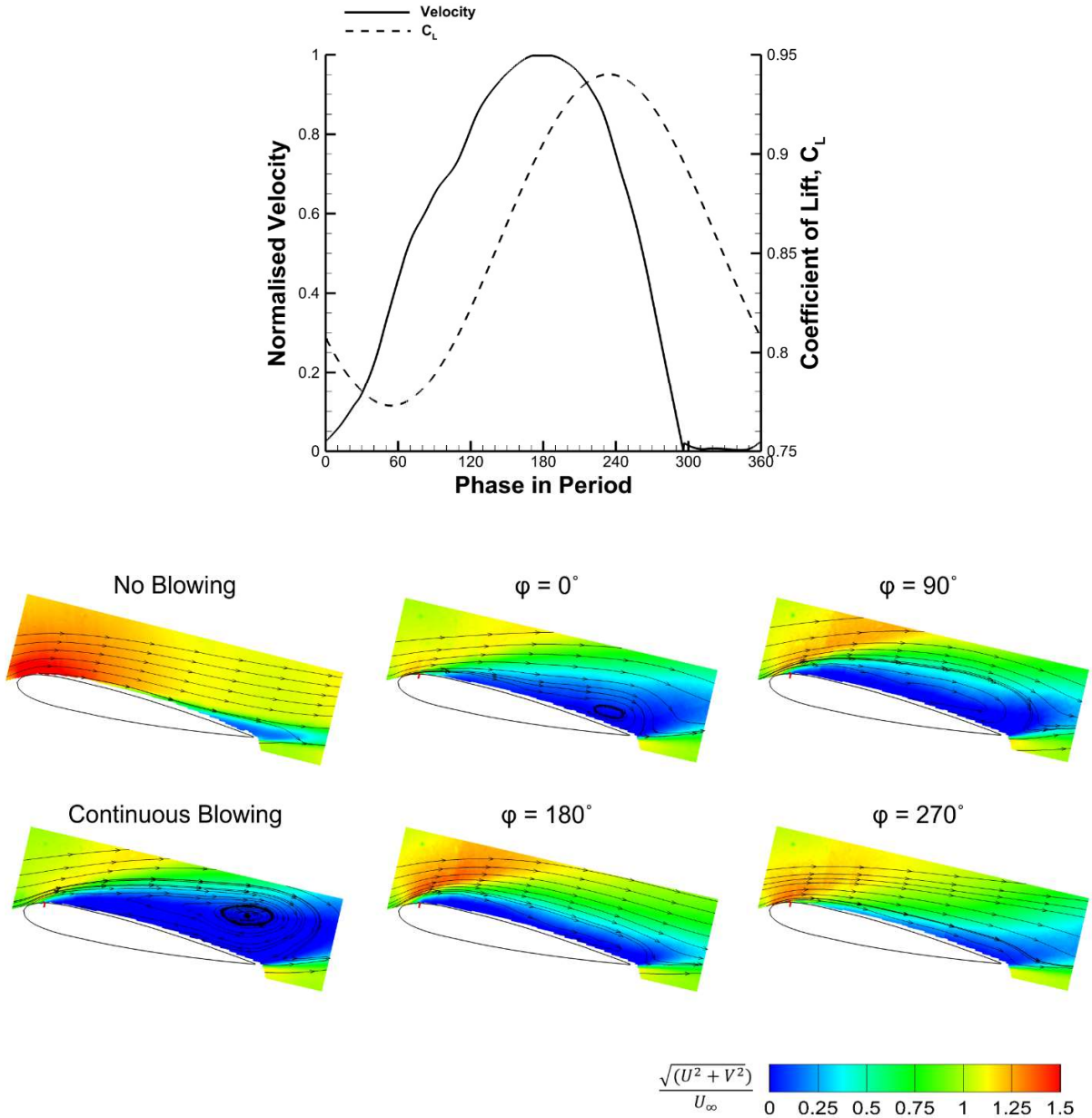

Figure 11. Phase-averaged velocity magnitude and streamlines at varying phases for k = 0.39, x_j/c = 0.08, and α = 13°.

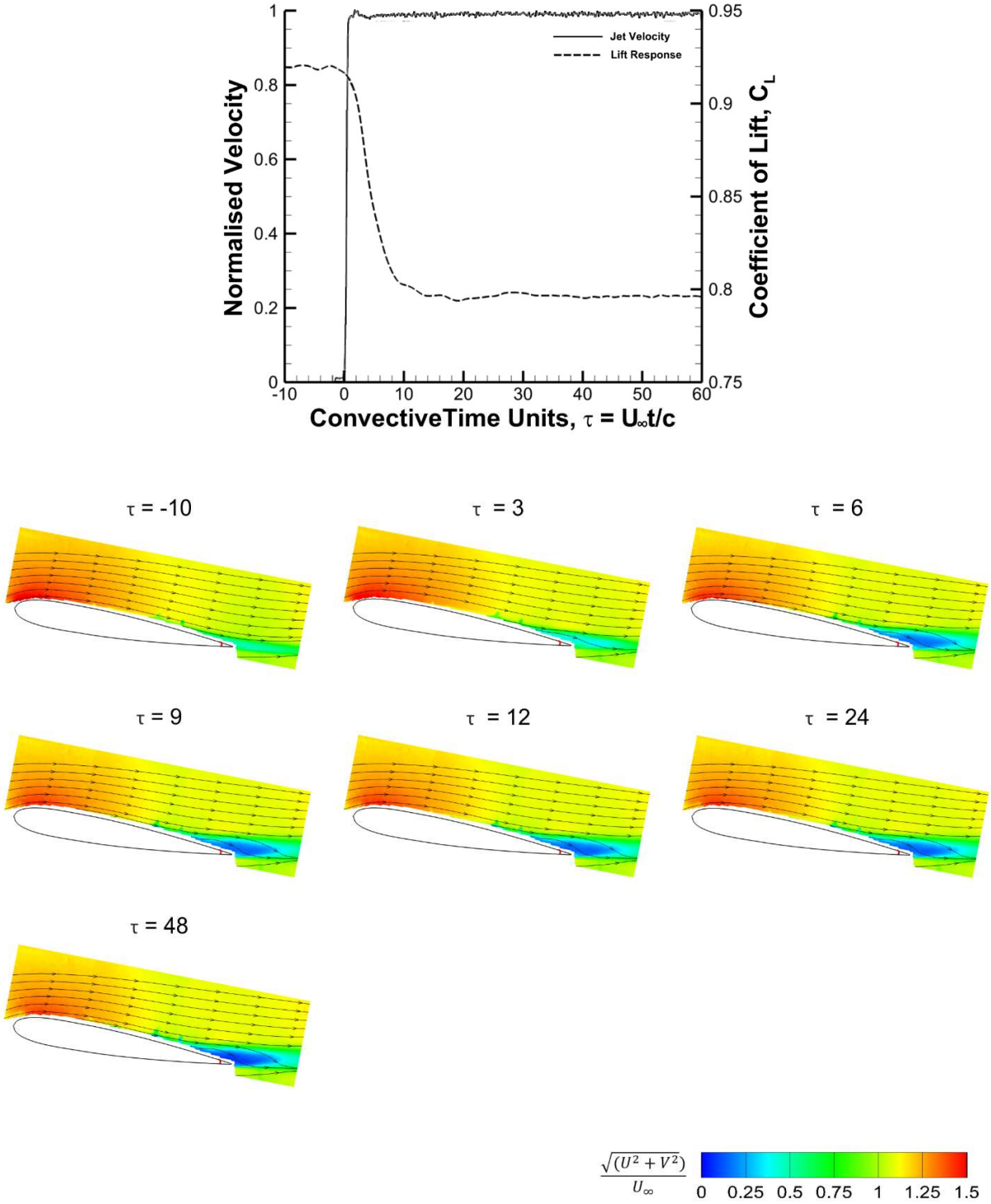

Figure 12. Phase-averaged velocity magnitude and streamlines at different instants for transient jet at x_j/c = 0.95 and α = 10°.

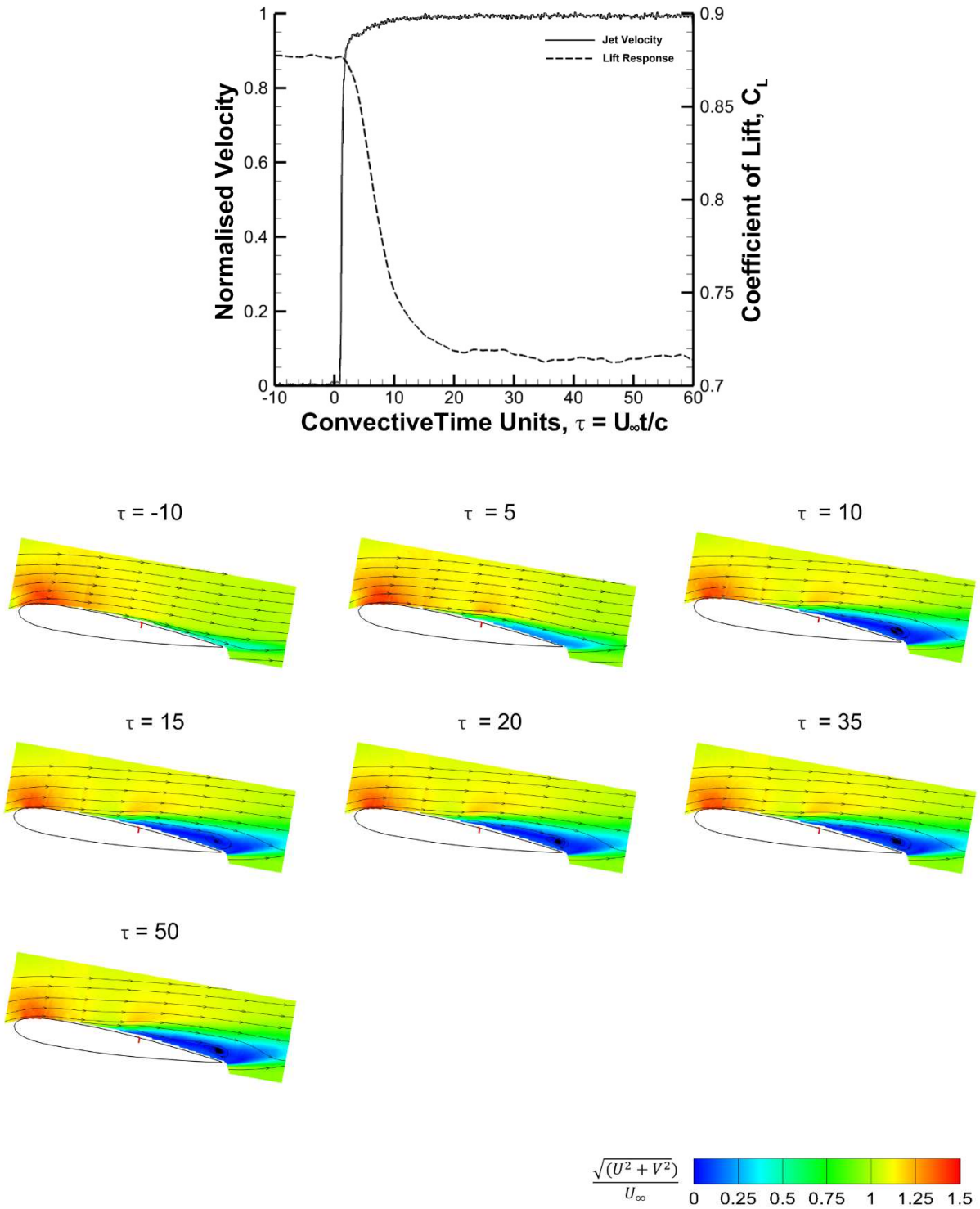

Figure 13. Phase-averaged velocity magnitude and streamlines at different instants for transient jet at x_j/c = 0.60 and α = 10°.

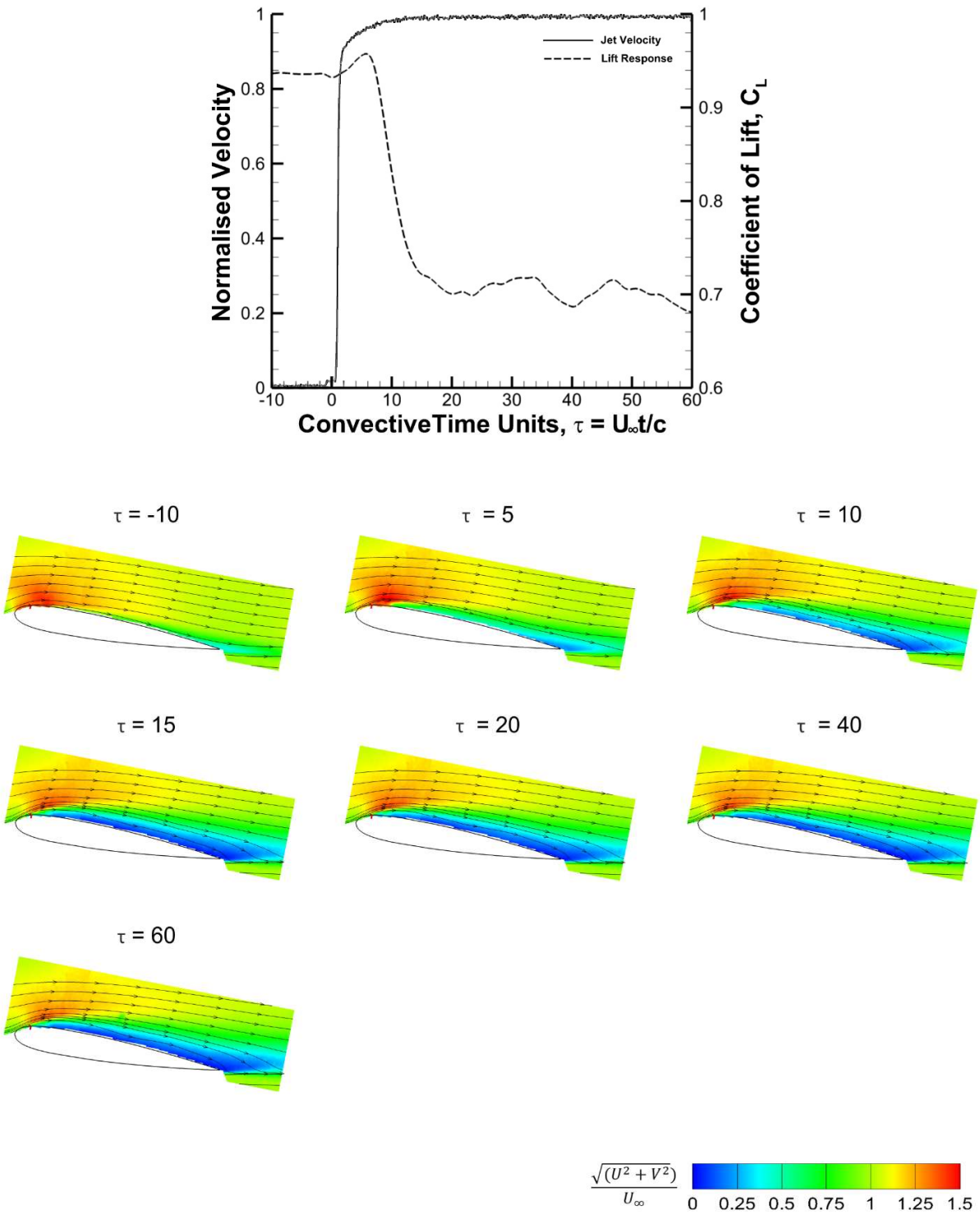

Figure 14. Phase-averaged velocity magnitude and streamlines at different instants for transient jet at x_j/c = 0.08 and α = 10°.

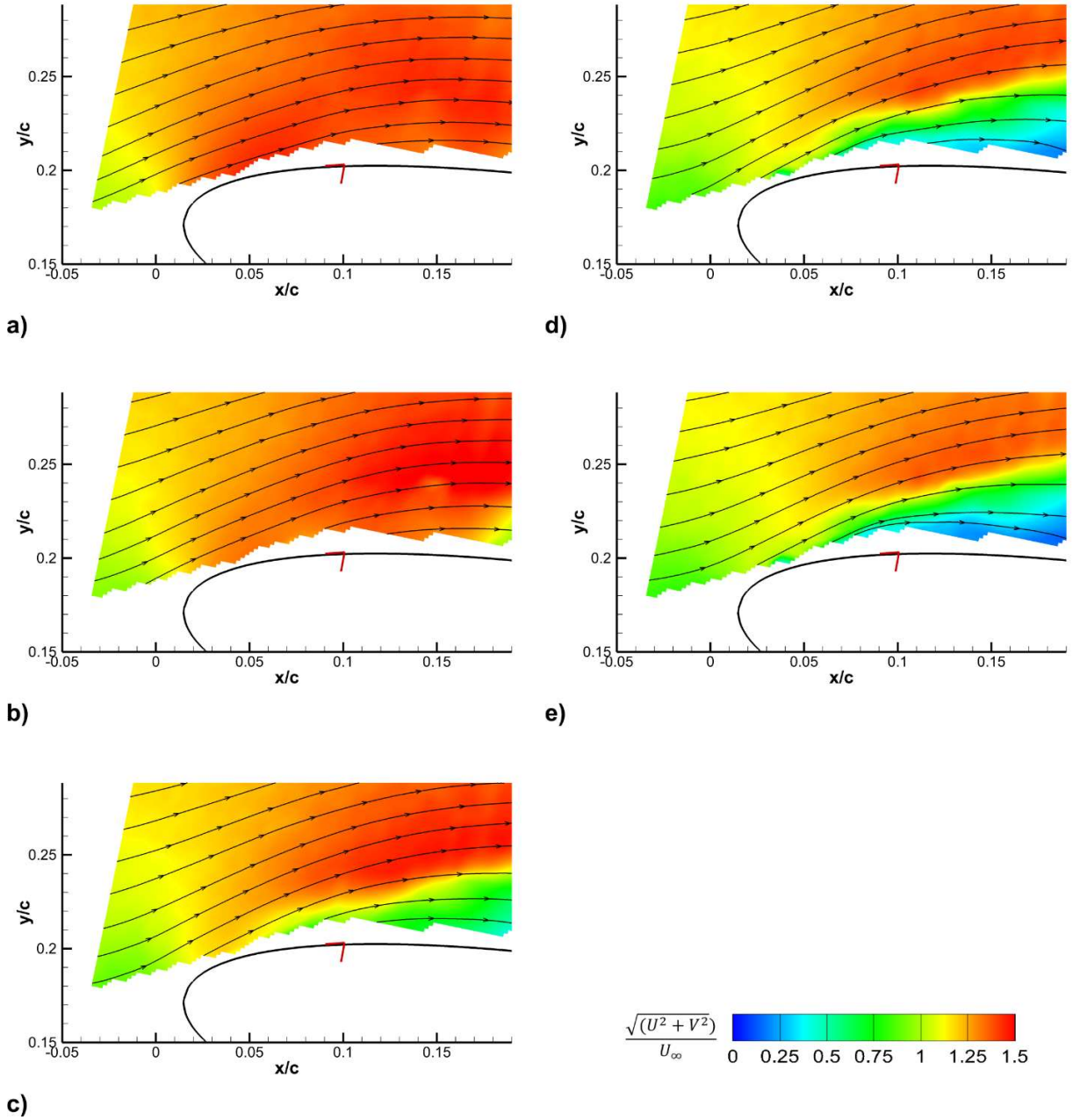

Figure 15. Velocity magnitude and streamlines at τ = -10, b) τ = 5, c) τ = 10, d) τ = 15 & e) τ = 60, for x_j/c = 0.08, α= 10°.

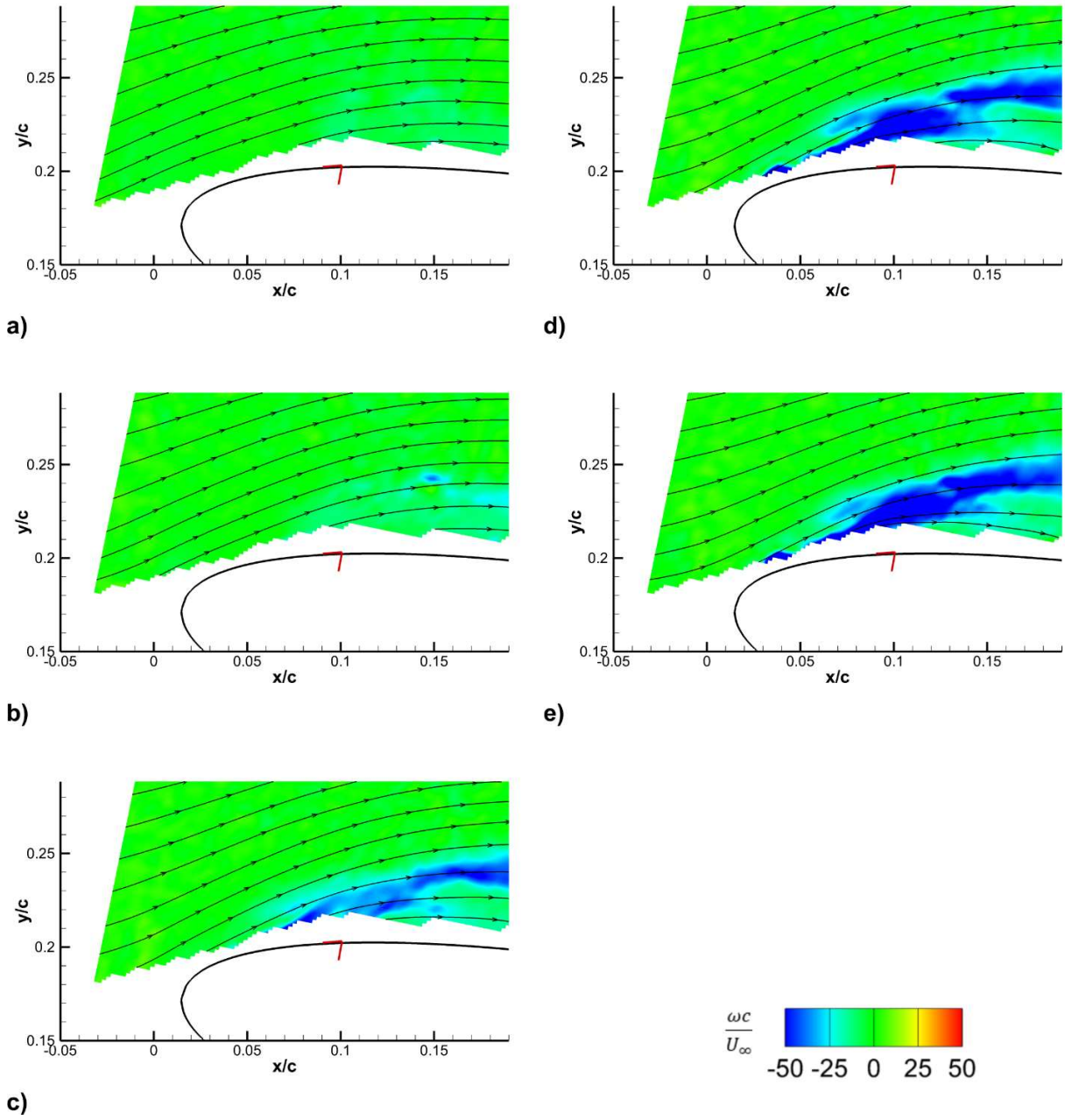

Figure 16. Vorticity magnitude at a) τ = -10, b) τ = 5, c) τ = 10, d) τ = 15 & e) τ = 60, for x_j/c = 0.08, α= 10°.

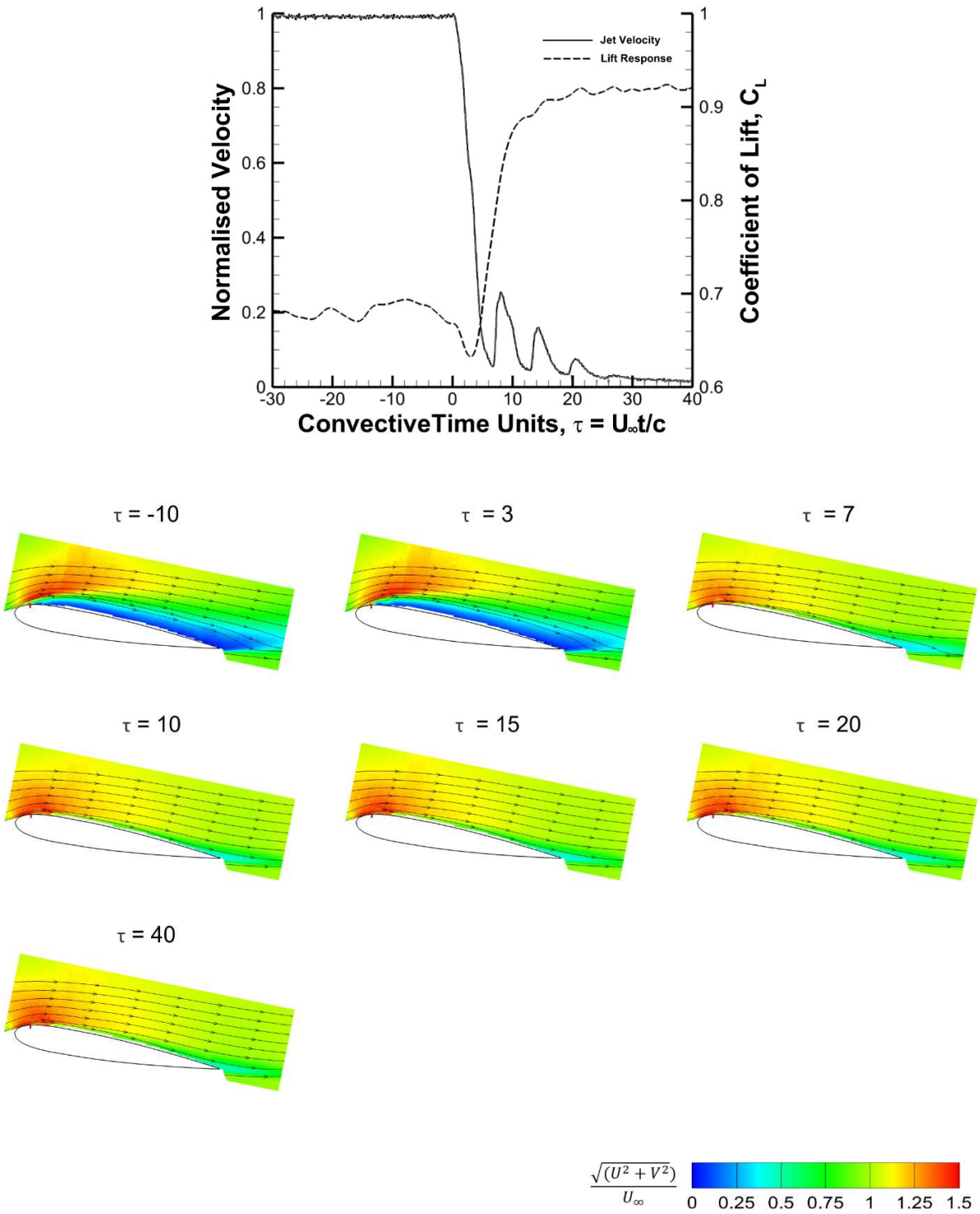

Figure 17. Phase-averaged velocity magnitude and streamlines at different instants for transient jet at x_j/c = 0.08 at α = 10°.

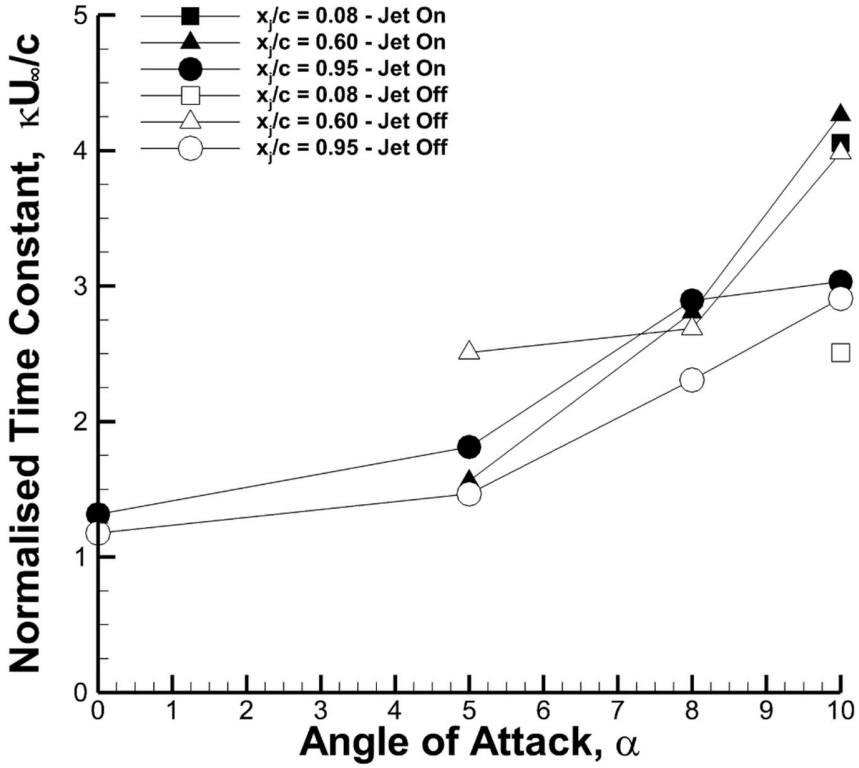

Figure 18. Estimated time constants for transient jets at x_j/c =0.08, 0.60 & 0.95.